

Effective Connectivity Maps in the Swine Somatosensory Cortex Estimated from Electrocorticography and Validated with Intracortical Local Field Potential Measurements

Masato Tanosaki,¹ Hideaki Ishibashi,² Tongsheng Zhang,³ and Yoshio Okada⁴

Abstract

Macroscopic techniques are increasingly being used to estimate functional connectivity in the brain, which provides valuable information about brain networks. In any such endeavors it is important to understand capabilities and limitations of each technique through direct validation, which is often lacking. This study evaluated a multiple dipole source analysis technique based on electrocorticography (ECOG) data in estimating effective connectivity maps and validated the technique with intracortical local field potential (LFP) recordings. The study was carried out in an animal model (swine) with a large brain to avoid complications caused by spreading of the volume current. The evaluation was carried out for the cortical projections from the trigeminal nerve and corticocortical connectivity from the first rostrum area (R1) in the primary somatosensory cortex. Stimulation of the snout and layer IV of the R1 did not activate all projection areas in each animal, although whenever an area was activated in a given animal, its location was consistent with the intracortical LFP. The two types of connectivity maps based on ECOG analysis were consistent with each other and also with those estimated from the intracortical LFP, although there were small discrepancies. The discrepancies in mean latency based on ECOG and LFP were all very small and nonsignificant: snout stimulation, -1.1 – 2.0 msec (contralateral hemisphere) and 3.9 – 8.5 msec (ipsilateral hemisphere); R1 stimulation, -1.4 – 2.2 msec for the ipsilateral and 0.6 – 1.4 msec for the contralateral hemisphere. Dipole source analysis based on ECOG appears to be quite useful for estimating effective connectivity maps in the brain.

Key words: current dipole source estimation; direct cortical stimulation; electrocorticography; evoked somatosensory potential; neuroimaging techniques; somatosensory cortical connectivity; somatosensory projection; trigeminal nerve

Introduction

BRAIN CONNECTIVITY IS actively being investigated using functional magnetic resonance imaging (fMRI) (Blatow et al., 2007; Friston, 2009; Friston et al., 2003; Stephan and Friston, 2010), electrophysiological techniques such as electrocorticography (ECOG), electroencephalography (EEG), and magnetoencephalography (MEG) (David et al., 2006; Gross et al., 2002; He et al., 2011; Kiebel et al., 2006; Kverga et al., 2011; Lin et al., 2009; Varela et al., 2001) and transcranial brain stimulations (Fox et al., 2012; Shafi et al., 2012). As cortical connectivity maps begin to produce

interesting new insights into the working of the brain, there is an increasing need to ascertain that the effective cortical connectivity maps estimated with noninvasive or quasi-noninvasive neuroimaging techniques correspond to actual maps in the brain (David et al., 2008; Logothetis, 2012; Ojemann et al., 2013).

Here we studied the capabilities and limitations of a multiple dipole source analysis technique in estimating effective connectivities based on ECOG data and validated the estimates using intracortical local field potential (LFP) recordings as gold standard. The effective connectivity has been studied classically by identifying the connected regions with evoked

¹Department of Neurology, Hachinohe City Hospital, Hachinohe, Aomori, Japan.

²Department of Neurosurgery, Asahikawa Medical University, Asahikawa, Hokkaido, Japan.

³Department of Neurology, University of New Mexico School of Medicine, Albuquerque, New Mexico.

⁴Department of Medicine, Boston Children's Hospital and Harvard Medical School, Boston, Massachusetts.

This work was performed at the University of New Mexico.

potential measurements and then measuring the latency of the initial response in each region. It can be also studied by measuring synchronized oscillatory activities between these regions (Brovelli, 2012; Brovelli et al., 2004; He et al., 2011; Lin et al., 2009). We estimated the connectivity based on a dipole source analysis of evoked ECOG data. The validation was carried out for the projections from the trigeminal nerve to the cerebral cortex and cortical forward connectivity from one dominant area in the primary somatosensory (SI) cortex to the other areas of the cortex. The study was carried out in an animal model (swine) with a large brain to avoid complications caused by spreading of the volume current. The somatosensory cortex occupies a disproportionately large portion of the cerebral cortex because of the importance of the snout in this species (Craner and Ray, 1991a,b; Okada et al., 1999).

Materials and Methods

Subjects

The experimental protocol was approved by the Animal Research Committee at the University of New Mexico Health Science Center. This report is based on experiments carried out on 19 anesthetized piglets (3–5 weeks old, 4–9 kg).

Surgical procedure

Each piglet was sedated with Telazol (8 mg/kg) i.m., and the ear vein was cannulated for intravenous injection of Fentanyl (0.1 mg/kg/h). A catheter was inserted into the trachea for artificial ventilation. The animal's head was secured in a custom-made head holder. The scalp was incised along the midline after local subcutaneous injection of 1% lidocaine, and the entire dorsal portion of the skull and dura were removed. The exposed cortical surface with intact pia was irrigated with saline. Heart rate and oxygen saturation were continuously monitored throughout each experiment. A bolus of Telazol or Fentanyl was given as needed based on the physiological monitoring during the measurements.

Gross anatomy of the somatosensory cortex of the swine

The trigeminal nerve innervating the snout projects to several cortical areas in each hemisphere (cf. Fig. 1) (Craner and

Ray, 1991a,b; Okada et al., 1999). These include the first rostrum area (R1) and second rostrum area (R2) of the SI cortex, and the secondary somatosensory (SII) cortex. The R1 is a large area that includes the coronal gyrus and adjacent sulcal areas of the cortex. It has a clear somatotopic representation of the contralateral snout with sulcus naris in the middle of the coronal gyrus corresponding to the nostril (Okada et al., 1999). The R2 is a smaller area in the cruciate gyrus anteromedial to R1. It receives input from the snout bilaterally (Craner and Ray, 1991a). The SII cortex is located in the sulcal and gyral walls of the suprasylvian cortex lateral to the coronal gyrus (Craner and Ray, 1991b). This area receives bilateral projections from the snout.

ECOG recordings

The ECOG recordings were carried out in six animals under both the snout and right R1 stimulation conditions. The left medial snout was stimulated with electric stimuli (50 μ sec, 3.0 mA, at 0.6 pulses/sec) delivered with a bipolar needle electrode. The epipial ECOGs were measured simultaneously at 106 locations with an array of silver ball electrodes \sim 1 mm in diameter and 4 mm apart (made from Teflon-insulated silver wires, 250 μ m bare diameter) placed over the exposed dorsal portion of the brain with the dura removed. The array was held by a plastic skull molded for each individual to fit its cortical surface with holes for the electrodes. Several holes were also present in the plastic skull for inserting the stimulating electrode for direct cortical stimulation.

Once the mapping was completed, the connectivity map from the R1 to other areas of the somatosensory cortex was determined in the same animal, using the same procedure as for the snout projection map. The cathode of the stimulating electrode (glass micropipette filled with 3 M NaCl, tip diameter 10–20 μ m) was placed in the layer IV of the R1 at the location receiving maximum projection from the snout. A small ring of thin silver wire was placed on the exposed cortical surface, concentrically around this micropipette electrode, to serve as the anode for focal bipolar stimulation. The depth of layer IV was defined as the depth at which the fastest thalamocortical volley with a negative LFP was found. All the ECOG data were recorded with a

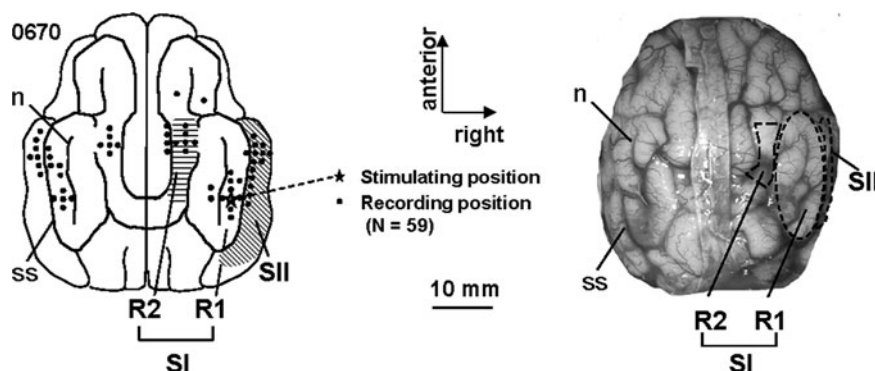


FIG. 1. Cerebral cortex of juvenile swine (example animal 0670). Stimulating (star) and recording (dots, $n=59$) electrode positions. Outline of the cerebral cortex reconstructed from a photograph. SI includes R1 and R2—nomenclature from Craner and Ray (1991a). Snout represented contralaterally and somatotopically around the coronal gyrus and the surrounding sulci and sulcus naris (n). R2 is in the sigmoid gyrus. SII is lateral to the coronal gyrus of R1 within and along the ss. SI, primary somatosensory; SII, secondary somatosensory; ss, suprasylvian sulcus.

bandwidth of 0.1–1,000 Hz and sampling rate of 10,000 Hz. Each average response was based on 30 epochs.

Localization of generators of ECOG data

As a prerequisite to the source analysis, the locations of all the recording and stimulation electrodes as well as the contour of the major sulci were determined with a magnetic positional tracking device (Polhemus FASTRAK) for each animal. Since the Polhemus transmits and receives magnetic field to determine this information, care must be taken to avoid distortions and biases caused by the presence of magnetic materials around the head of the animal such as the stereotaxic headholder. We used in-house software to monitor the position of the stylus of the Polhemus online, displayed on a monitor in 3D. For each electrode, we collected 100 samples continuously and values greater than 1.2 and less than 0.8 relative to the mean were rejected as outliers (because of, e.g., the orientation of the stylus relative to the magnetic metals). The average position was computed from the accepted values. The estimated values were double-checked by comparing these values with the values obtained with a tape ruler. The differences were generally < 1 mm.

The source analysis was carried out with BESA software (Megis). An isotropic homogeneous sphere was fit to the brain surface determined by the digitized ECOG electrode locations. The sphere was placed within the x - y - z coordinate system conventionally used for EEG and MEG analysis in which the x -axis goes from the left to the right ear, the y -axis is orthogonal to the x -axis, pointing to the nose, and the z -axis is orthogonal to the x - and y -axis, pointing to the vertex. The center of the best fitting sphere was placed at the origin of this coordinate system. All the electrode location data were transformed into this new coordinate system. The data from 106 ECOG electrodes were converted to a BESA-compatible data format. If there were bad channels (e.g., because of poor electrical contact with the pial surface), we estimated their values using a spline interpolation with Legendre polynomials of order 10 based on 10 closest neighbors.

We then transformed the ECOG data into a Laplacian map. The Laplacian map was obtained by taking the second spatial derivative of the evoked potential along the two orthogonal directions on the cortical surface. The peaks in the map correspond to the areas where there is a maximum current inflow or outflow from the cortical surface below each peak. The Laplacian maps were spatially sharper than the raw ECOG maps, and thus they facilitated the identification of the active cortical areas for both the snout and R1 stimulations.

In our initial source analysis we used the genetic dipole fitting function available in BESA to locate the dipole sources. The genetic algorithm is an optimization strategy based on evolutionary processes. It creates a population of individuals and each individual represents one solution. The source number was set to the number we found from the surface Laplacian analysis. Then, the source information, including dipole strength, locations, and directions, was output. We found from this initial analysis that a one-step simultaneous fitting of the data at all 106 locations distorted the source localization results because of a dominant strong response in the right R1, especially for the data obtained with direct cortical stimulation.

We thus used a two-step procedure to estimate the multiple sources. Once the peaks were identified from the Laplacian map, a single equivalent current dipole (ECD) was placed within the region of each peak including up to 10 electrodes and then the genetic algorithm was used to determine its location and orientation within the time window of peak amplitude with a constraint that there is only one ECD in the region. We then used the genetic algorithm to estimate the orientation and source waveform of the ECDs located in the region of each peak in the Laplacian map. The number of ECDs was set to the number corresponding to the number of peaks in the Laplacian map. The location of each ECD was fixed at the location determined in the first step, while the orientation was free to vary. The source fitting was carried out using the data from all 106 electrodes.

An inverse transformation and rotation matrix was then applied to the result using our in-house software in order to project the sources onto the piglet cortex. The strength is represented by the length of the dipole and the direction by the color, with red representing the dipole's positive side and blue representing the negative side. The onset latency was defined as the time at which the source waveform deviated from the baseline.

Intracortical LFP recordings

The projection from the snout to the cortex and cortico-cortical connectivity from the R1 were determined with the intracortical LFP recordings in order to validate the maps estimated from the ECOG source analysis. In one set of experiments, the snout and R1 maps were obtained from each of four animals. The stimulation methods used for the ECOG analysis were used. The recording electrode was same as the stimulating glass micropipette with the reference electrode placed on the retracted scalp. When a reliable response was detected at a given cortical location, multiple electrode recordings were obtained with a 1–2 mm spacing on the cortical surface to delineate the active tissue area, the area in which the LFP was more than half the maximum amplitude at a particular depth. The recording electrode was inserted into the cortex at the center of activity as perpendicular to the cortical surface as possible and LFPs were recorded in 0.5 mm increments from the cortical surface to the depth of 2.0 mm. There were two types of laminar profiles: (1) the LFP reversed vertically along the cortical lamina in one case, which was interpreted to be caused by a vertically oriented cortical current generator in the gyrus; (2) in the second case, the polarity reversal was seen across along the transverse direction parallel to the cortical surface, which was interpreted to be caused by a horizontally oriented current generator perpendicular to the sulcal wall. The depth of the vertically oriented generator was defined as the shallowest recording position at which the negative potential was found. The depth of the horizontally oriented generator was defined as the average of the depths at which the negative and positive potentials were at their maximum. The LFPs were recorded with the same parameters as for the ECOG.

In another set of experiments, the connectivity map for the R1 was determined in a larger number of animals ($n=9$) to establish the reliability of the map based on intracortical LFP. The stimulation and recording procedures were the

same as above. Figure 1 shows the recording electrode locations for one animal (No. 0670) in this series. Once a peak of activity was found, the depth profile of the evoked potential was determined. The mean depth corresponded to the layer IV determined histologically in our previous study (Ikeda et al., 2002).

The onset latency of the initial response was defined in all cases as the time at which the first component with polarity reversal deviated from the baseline. In some recordings there was an earlier component without any synaptic delay and without any polarity reversal across depth. This was interpreted as volume conducted from the response evoked electrically without any synaptic delay by the stimulating electrode; consequently, they were disregarded in estimating the forward effective connectivity latencies.

Connectivity analysis

The connectivity maps from the snout and from the right R1 were determined simply based on the onset latency of the evoked response at each projection site. The connectivity maps for each type of stimulation were estimated separately based on the ECOG source analysis and LFP latency measurements. The connectivity maps based on the ECOG are based on the onset latency of the initial component of

the source waveform at each projection site as defined above in the section Localization of generators of ECOG data. The connectivity maps based on the LFP are based on the onset latency of the initial synaptically mediated component as defined in the section Intracortical LFP recordings.

Results

Cortical projection and connectivity maps identified with ECOG

Trigeminal nerve (snout) stimulation. Snout stimulation activated 2–5 cortical areas in the six animals studied. The number of areas activated varied across the animals, but it was reproducible across animals whenever they were detected. Figure 2 shows the results for one animal with five identified active areas. Figure 2A shows a superimposed set of ECOG waveforms. Figure 2B shows the surface Laplacian map on the pial surface at 60 msec after snout stimulation. A source analysis was carried out to identify the location, orientation, and waveform of each current source in the cortical network activated by the stimulation (Fig. 2C). The source locations are shown on the outline of the electrode array and cortex of this animal. These locations

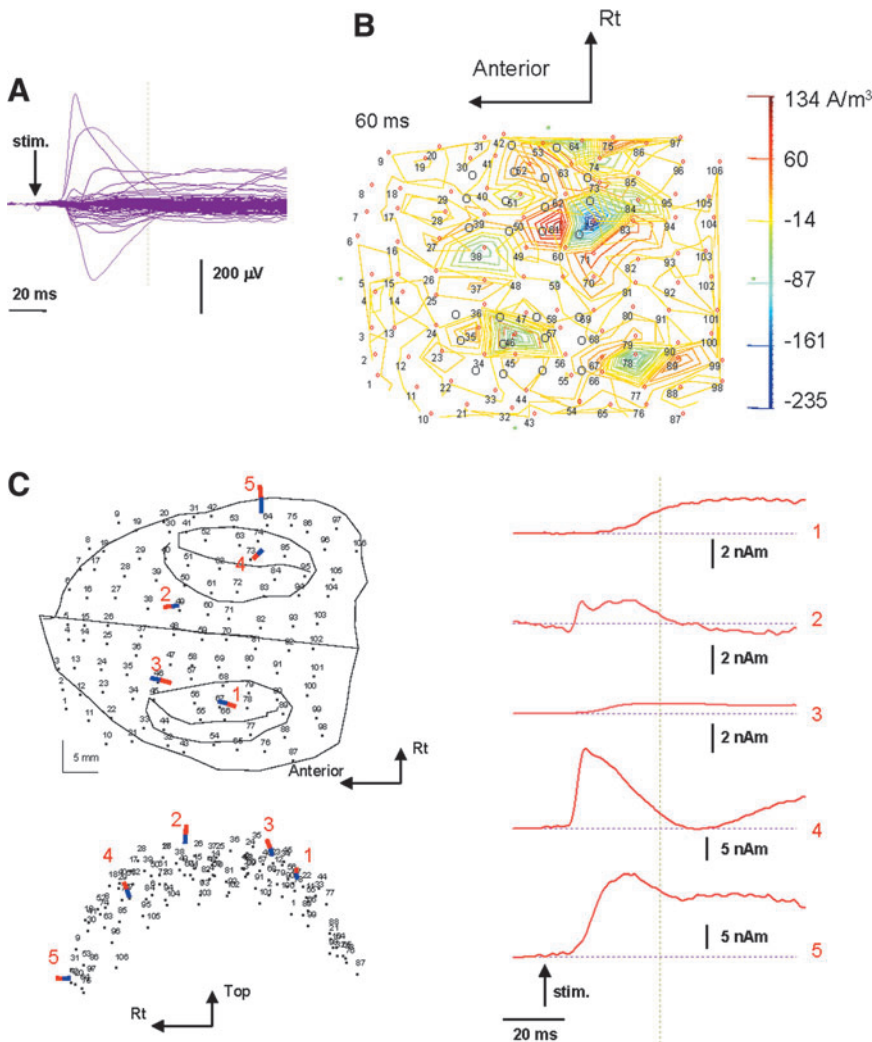


FIG. 2. Epipial ECOG signals elicited by left snout stimulation and cortical sources estimated from the ECOG data. Electric stimuli to the left medial snout. ECOGs were simultaneously measured with 106 electrodes placed on the epipial cortical surface. (A) Superimposed ECOG waveforms for the 106 channels. (B) Surface Laplacian map 60 msec post-stimulus. (C) Dipole source analysis. Location and orientation of each ECD shown by a bar. Each dipole is located in the midpoint, and directed toward the red side. Left: Locations of five sources are superimposed on the horizontal and coronal views of the electrode array and an outline of the exposed cortex determined with Polhemus FAS-TRAK. Right: Waveforms of the five sources. ECD, equivalent current dipole; ECOG, electrocorticography.

correspond to the peak areas in the Laplacian map. The source waveforms are also shown in Figure 2C. The left snout stimulation activated the contralateral R1 most strongly (source 4 near electrode 73 with a strong bipolar peak in the Laplacian map). The stimulation also activated the contralateral R2 (source 2 near electrode 49 with a monopolar peak) and SII (source 5 near electrode 64 with a bipolar peak). The ipsilateral activation was seen in left R2 (source 3 near electrode 46 with a monopolar peak) and in left R1 (source 1 near electrode 78 with a monopolar peak).

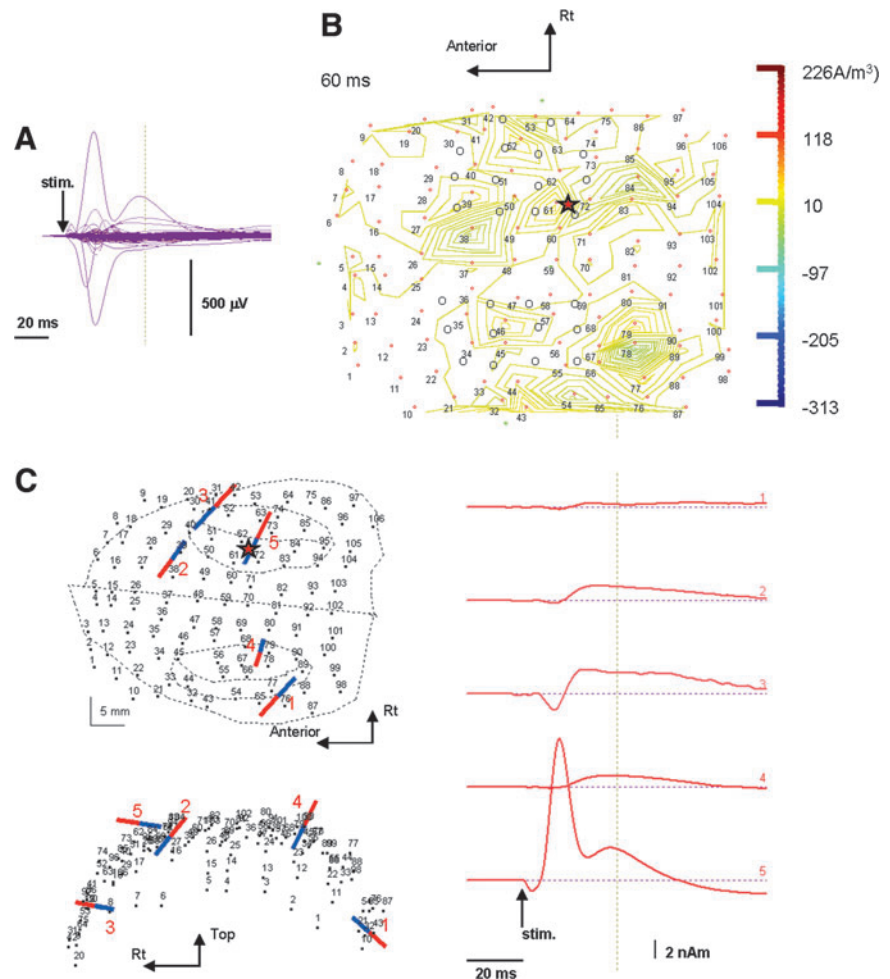
An analysis of the time course of activation based on the Laplacian map (not shown) showed (1) initial peak response clearly seen at 15 msec, (2) differentiating into activation of R1 and R2 in the right cortex between 15 and 20 msec, (3) activation of right SII by 30 msec, and (4) ipsilateral responses starting at 40 msec in left R1 and R2. Right R1 and R2 responses were detected in all six subjects, while right SII responses were seen in two subjects. Left R1 response was detected in two subjects, whereas left R2 activity was observed in three subjects. The activation of left SII cortex was not seen in this animal because of the limited coverage of the electrode array, but it was seen in $n=2/6$ subjects. The source waveforms showed strong and fast activation in right R1 (No. 4), weaker but fast activation in right R2 (No. 2), stronger but delayed activation in right SII (No.

5), very small activation in left R2, and clear but delayed activation in left R1. Left SII activity was not localized in this animal, but was localized in 2/6 animals.

Direct cortical stimulation of R1. The R1 stimulation activated 1–5 cortical areas in the six animals studied. The number of areas activated varied across the animals as for the snout stimulation. Several areas were activated in all animals except one, in which the activation was observed only at around the stimulating electrode in right R1. In all cases, when focal evoked potential was seen in a given area on the pial surface, that location was comparable to the location found with the intracortical LFPs described below. Figure 3A shows the superimposed ECOG waveforms evoked by stimulation of the R1 at the location indicated by a star in Figure 3B and C. Figure 3B shows the Laplacian map for this subject with five active areas at a latency of 60 msec after stimulation. Figure 3C shows the results of the dipole analysis. The five ECDs are shown in the horizontal and coronal views of the electrode array and exposed cortex. Figure 3C also shows the source waveforms.

The R1 stimulation at the location indicated by the star produced a strong source in the R1 (source 5 near electrode 62 with a bipolar peak) with the initial component having no synaptic delay and short-latency components. The R1 stimulation produced short-latency activation of right R2 (source 2

FIG. 3. Epipial ECOG signals elicited by direct electric stimulation of the layer IV of the right R1 cortex. Stimulation point, red star in (B) and (C). (A) Superimposed ECOG waveforms for the 106 channels. (B) Surface Laplacian maps at 60 msec post-stimulus. (C) ECD position and orientation (left) and source waveforms (right). Left R2 source seen in (B) was not identified by the dipole analysis.



near electrode 38 with a bipolar peak in Fig. 3B) and right SII (source 3 near electrode 41 with a bipolar peak). The stimulation also produced clear activity in the contralateral left R1 (source 4 near electrode 78 with a bipolar peak) and weak activity in left SII (source 1 near electrode 76 with a bipolar peak). Weak activity was seen in left R2 in the Laplacian map near electrodes 46, 47, and 57, but it was too weak and ill-organized to be detected by the dipole analysis.

Validation of the cortical projection and connectivity maps based on intracortical LFP

Trigeminal nerve (snout) stimulation. In this study with four animals, the snout was stimulated using exactly the same protocol as for the ECOG study above. Evoked responses were measured with intracortical LFP over the entire somatosensory cortex, searching for reliable LFP with polarity reversal across cortical layers. Snout stimulation activated 3–5 cortical areas in the four animals studied. The number of areas activated varied across the animals, but each area was reproducibly activated in at least two animals.

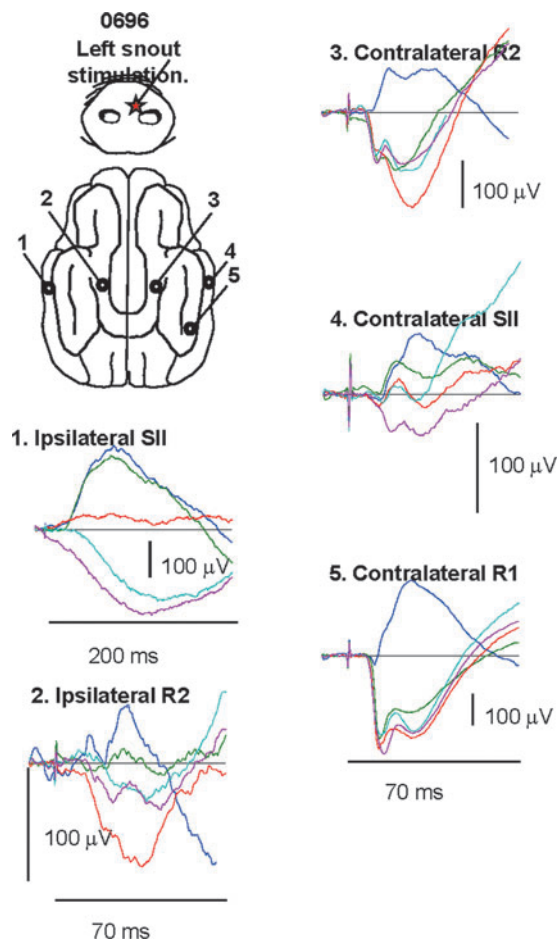


FIG. 4. Intracortical LFPs elicited by the snout stimulation (location shown by red star in animal 0696) in various regions of the somatosensory cortex. Stimulation elicited responses in left SII (1), left R1 (2), right R2 (3), right SII (4), and right R1 (5). These potentials showed focal activation with clear polarity reversals across the cortical layers in each area. LFP, local field potential.

Figure 4 shows the data from one animal in which all five areas were activated by the snout stimulation. These potentials show clear polarity reversals across the cortical layers, indicating that the stimulation activated each of these areas. LFPs were elicited in the contralateral right R2 (location 3), SII (location 4), and R1 (location 5) and in the ipsilateral left SII (location 1) and R2 (location 2). There was no clear polarity reversal in the left R1.

The cortical projection from the snout is shown in Figure 5. Figure 5A summarizes the group results for four animals. The upper row of Figure 5B shows the individual results. The snout projected to very similar locations in the R1, R2, and SII of the contralateral right hemisphere across the animals, except for the very posterior activation of SII in animal 0697. The activation in the ipsilateral left side was seen in R2 in 3/4 of the animals, in SII in 2/4, and none in R1. This pattern is consistent with the results based on ECOG, except for the lack of ipsilateral left R1 activation.

Direct cortical stimulation of R1. The R1 stimulation activated 4–5 areas in all 9 animals studied. Figure 6A shows the results for one animal. There are evoked responses in the three cortical areas (right R1, R2, and SII) ipsilateral to stimulation. Activation in the R1 ($n=9/9$) was distributed over the lateral portion of the coronal gyrus and lateral to the sulcus naris, and was localized within 2 mm surrounding the stimulation site. The response waveforms were very complex and varied significantly with recording electrode position. The response near the stimulating electrode contained a very sharp response without synaptic delay, followed by complex variation of the waveform across layers (location a in Fig. 6A). Activation of the R2 region ($n=7/9$) was localized in the cruciate gyrus and its adjacent sulcus, medial to the coronal gyrus of R1, within 2.0 mm in any direction from the peak. The waveforms in the R2 (location b maximum response) consisted of an initial response without polarity reversal across the cortical layers, followed by a component whose amplitude varied across the depth. The responses were generated in the sulcus ($n=5/7$) and gyrus ($n=2/7$). Activation was found in right SII (area c) ($n=8/9$). The center of activity was located within the cortex lateral to the anterior half of the rostral suprasylvian sulcus. The waveform at response maximum (location c) consisted of an initial component that did not reverse its negative polarity across the depth. As for the initial component of the response in the R2, this component decreased as a function of the distance from the stimulation point, indicating it was generated outside SII, attributable to the intracortical spread of the ipsilateral R1 response because of volume conduction. Its spatial extent was rather widespread, probably owing to unexpectedly strong evoked potentials in the adjacent R1. This initial component was followed by the second component, which showed polarity reversal at the depth of 1.3 ± 0.6 mm ($n=8$). The region of polarity reversal was confined to a small volume of tissue <4 mm in any direction.

Stimulation of the right R1 elicited cortical potentials in the contralateral left R1 in all nine animals (Fig. 6B). The responses from one animal were distributed along the anterior–posterior direction, but sharply attenuated along the coronal plane. The maximum response was seen at position “a.” The responses were generally confined to a focal area of ≤ 4 mm in any direction among all animals. Cortical potentials in the

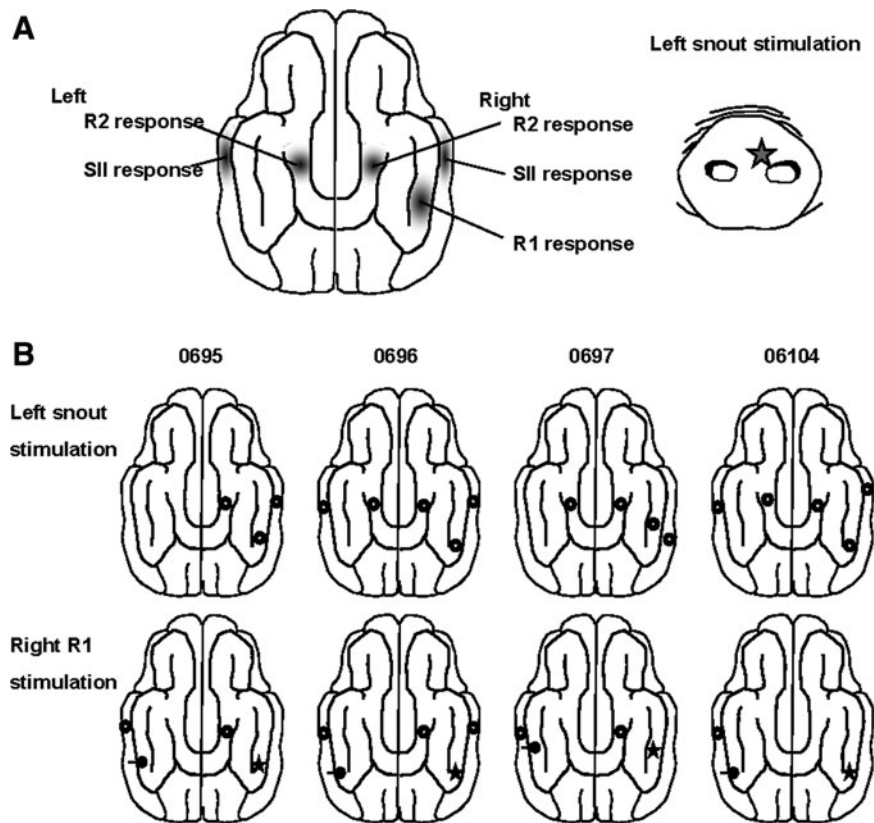


FIG. 5. Projection maps for the trigeminal nerve (snout). **(A)** Group summary of the connectivity map. Stimulation activated the contralateral right R1, R2, and SII, and ipsilateral left R2 and SII. **(B)** Top row: individual data of the four animals studied. Bottom row: maps of corticocortical connectivity from right R1 (at the location of maximum projection from the same snout position) in the same animals. Although the number of activated sites was variable across the animals, any given projection area when activated was very similar between the snout and R1 stimulation conditions.

R1 were generated by underlying currents directed vertically from the deep layers to the cortical surface in 6/9 animals and by horizontal currents in 3/9 animals. Activation of the left SII was seen in 8/9 animals. The maximum response for one animal was at location b. The region of active tissue did not extend beyond 4.0 mm in any direction and was located in the crown of the gyrus lateral to the anterior half of the rostral suprasylvian sulcus in the contralateral hemisphere. The onset latency of the initial component was 11.2 ± 3.3 msec, which was significantly longer than that of the contralateral R1 response of 7.5 ± 1.3 msec (paired *t*-test, $p < 0.01$). The locations of the ipsi- and contralateral SII responses were highly symmetrical in 5/7 animals in which bilateral activation was found. There was no clear polarity reversal in the left R2.

The cortical areas receiving forward projections from the right R1 cortex are summarized in Figure 7. As illustrated in Figure 7A, the group data indicated that there were forward connections from the right R1 to the ipsilateral R2 and SII and contralateral R1 and SII. However, there was no clear-cut connection to the contralateral R2. The individual connectivity maps are shown in Figure 7B. A visual comparison of Figure 7A and B shows that the maps for the individual animals are quite similar to the map for the group data. When a particular area was activated in a given animal, that area matched in location with the area shown for the group data. It is unclear why evoked responses were not uniformly detected in all the five cortical areas in every animal. The connectivity map based on the intracortical LFP is consistent with the map based on the ECOG. The activity in left R2 was detectable

in some cases based on ECOG, but it was too weak and ill-organized to be detected by the dipole source analysis, thus consistent with the intracortical LFP result.

Direct comparison of the cortical projection and connectivity maps for R1 determined with intracortical LFP. As part of the study described in the section Trigeminal nerve (snout) stimulation, we determined the cortical projection maps for the snout and cortical connectivity maps for R1 in the same four animals in order to eliminate individual and experimental variability across animals. The maps for the R1 stimulation were determined exactly as in the previous study (the section Direct cortical stimulation of R1). The individual data in Figure 5B show the cortical projection maps based on snout stimulation and cortical connectivity maps for right R1 for each animal. Again, there is a large variability in the number of projection sites activated across animals, but whenever a given area was activated, its location was quite similar across the animals. As noted already, the snout stimulation did not produce any clear polarity reversal in the left R1 based on the intracortical LFP measurements, but the right R1 stimulation reliably activated the left R1. The snout stimulation activated left R2, but the right R1 did not. Notwithstanding these differences, there was a high degree of consistency in the projection areas when any given area was activated by both the snout and R1 stimulations. Whenever a given area was activated by the two types of stimulation, the location of activity was very close to each other across the two maps (mean difference = 0.8 ± 1.4 mm). We conclude from these results that the location in the right R1 receiving the maximum

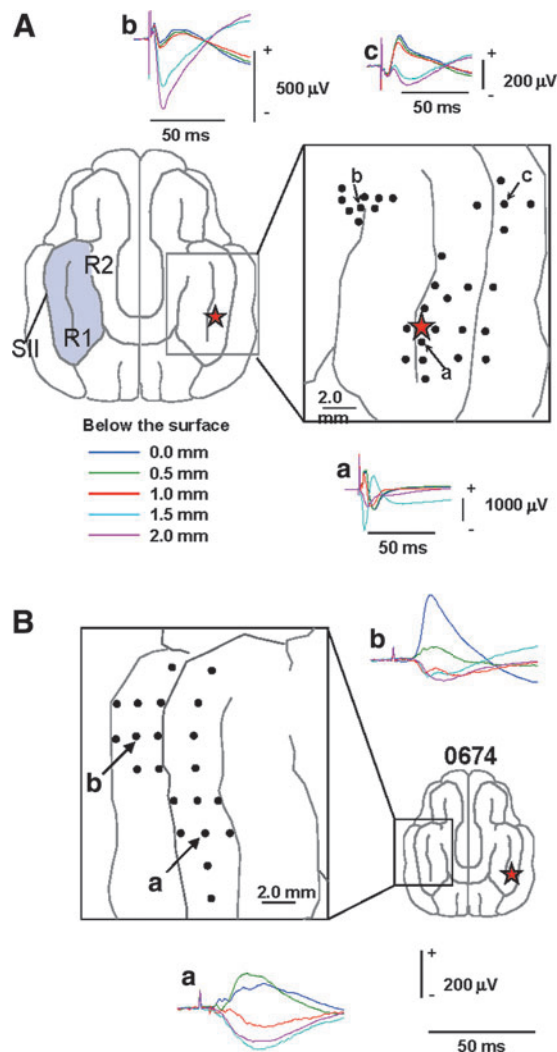


FIG. 6. Intracortical LFP elicited by stimulation of the layer IV of the right R1 (shown by red star) in various regions of the somatosensory cortex. LFPs were recorded at the positions indicated by dots, along the cortical lamina at the depths from 0.0 to 2.0 mm with 0.5 mm at each position. LFP waveforms are shown at the peak location in each area. **(A)** Responses in the hemisphere ipsilateral to stimulation. **(B)** Responses in the hemisphere contralateral to stimulation. Note polarity reversal along the cortical depth at each projection area.

projection from the snout projects to those areas that are indistinguishable from the areas receiving projections directly from the snout stimulation.

Cortical projection from snout and connectivity map from R1. Table 1 shows the onset and peak latencies as well as dipole moment of the initial response in the estimated source waveforms in the six nodes of the network based on the ECOG study with six animals. The latencies of initial cortical activation in the contralateral right hemisphere estimated with the ECOG source waveforms were remarkably similar to those determined with the intracortical LFP from another study with four animals. The latencies were consistently longer compared with the intracortical LFP, but the differences

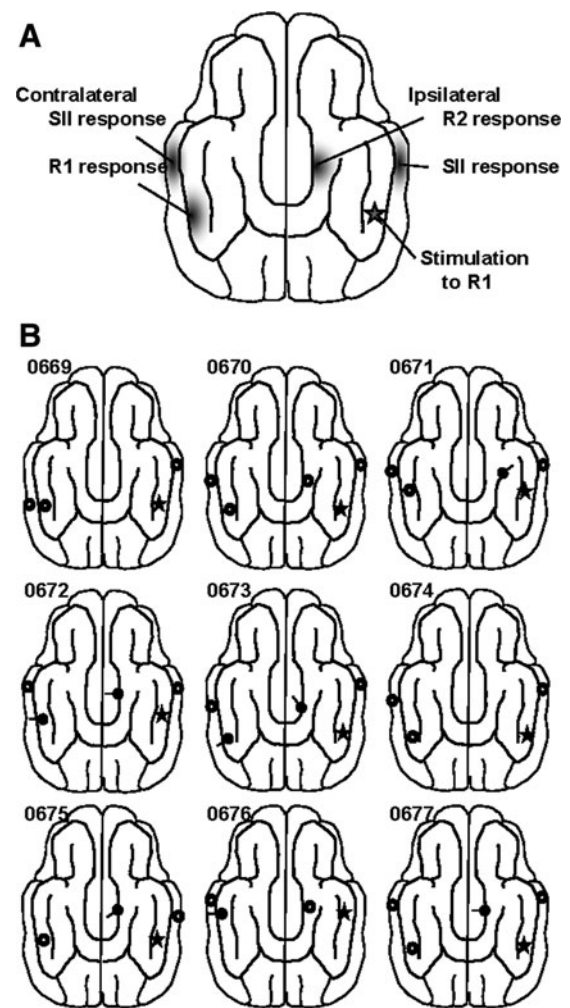


FIG. 7. Forward corticocortical connectivity map originating from right R1. **(A)** Connectivity map for the group. Electric stimulation in right R1 cortex (star) activated ipsilateral R2 and SII, and contralateral R1 and SII. **(B)** Connectivity maps for individual animals ($n=9$). Star shows the stimulation site for each animal. Open circles indicate activation sites with vertically oriented cortical currents directed from the deep cortical layers toward the cortical surface. Filled circles with a stick indicate the activation site with horizontally directed currents, probably located in the sulcus. Although not all four areas were activated in any given animal, the active site closely matched the group data when a given area was activated.

were quite small, that is, +1.2, +2.0, and +1.1 msec for right R1, R2, and SII, respectively. These differences were not statistically significant according to t -test at $p>0.05$. The discrepancies for the ipsilateral left cortex were somewhat larger for the ECOG estimates (+3.9 and +6.3 msec for left R2 and SII, respectively). However, the pattern of the latencies is consistent with the pattern found with the intracortical LFP. The differences in mean latency for left R2 and SII were not significant (t -test, $p>0.05$). One discrepancy was noted between the projection maps determined with ECOG and LFP; that is, the ipsilateral R1 activation was seen with ECOG but not with LFP. The dipole moment Q for left R1 shown in Table 1 indicates that this discrepancy

TABLE 1. PROJECTION LATENCIES AND DIPOLE MOMENT OF THE FIRST COMPONENT OF THE SOURCE WAVEFORM OF THE ACTIVITY ELICITED BY LEFT MEDIAL SNUOT STIMULATION, ESTIMATED FROM THE EPIPIAL ELECTROCORTICOGRAPHY AND COMPARISON WITH PROJECTION LATENCIES DETERMINED WITH INTRACORTICAL LOCAL FIELD POTENTIAL

Left snout stimulation	Area	ECOG	Intracortical LFP
Onset latencies (msec)	Lt SII	17.5±4.1 n=2	26.0±6.0 n=2
	Lt R2	12.7±5.8 n=3	8.8±1.4 n=3
	Lt R1	14.7±6.4 n=2	
	Rt R2	9.1±1.4 n=6	7.1±2.9 n=4
	Rt R1	8.4±1.1 n=6	7.2±1.7 n=4
Peak latencies (msec)	Lt SII	71.7±31.2 n=2	
	Lt R2	58.8±17.2 n=3	
	Lt R1	83.7±5.2 n=2	
	Rt R2	23.6±9.1 n=6	
	Rt R1	24.5±13.5 n=6	
Dipole moment (nAm)	Lt SII	2.8±0.2 n=2	
	Lt R2	1.2±0.5 n=3	
	Lt R1	1.8±0.8 n=2	
	Rt R2	3.7±3.6 n=6	
	Rt R1	7.2±6.1 n=6	

ECOG, electrocorticography; LFP, local field potential; Lt, left; Rt, right.

may not be large. The reliable response was detected only in 2/6 animals and the value of Q was only 1.8 ± 0.8 nAm according to the ECOG analysis. This weak response is consistent with the lack of polarity reversal at this location in the intracortical LFP data.

TABLE 2. PROJECTION LATENCIES AND DIPOLE MOMENT OF THE FIRST COMPONENT OF THE SOURCE WAVEFORM OF THE ACTIVITY ELICITED BY RIGHT R1 STIMULATION, ESTIMATED FROM THE EPIPIAL ELECTROCORTICOGRAPHY AND COMPARISON WITH PROJECTION LATENCIES DETERMINED WITH INTRACORTICAL LOCAL FIELD POTENTIAL

Right R1 stimulation	Area	ECOG	Intracortical LFP
Onset latencies (msec)	Lt SII	10.6 n=1	11.2±3.3 n=8
	Lt R1	8.9±1.8 n=4	7.5±1.3 n=9
	Rt R1	0 n=6	
	Rt R2	6.9±1.1 n=4	5.5±1.2 n=7
	Rt SII	8.0±0.3 n=2	5.8±1.4 n=8
Peak latencies (msec)	Lt SII	21.0 n=1	
	Lt R1	22.1±6.9 n=4	
	Rt R1	10.7±8.3 n=6	
	Rt R2	20.5±8.2 n=4	
	Rt SII	27.6±11.0 n=2	
Dipole moment (nAm)	Lt SII	0.53 n=1	
	Lt R1	1.2±0.5 n=4	
	Rt R1	23.1±12.1 n=6	
	Rt R2	2.8±1.7 n=4	
	Rt SII	5.6±5.1 n=2	

Table 2 shows the onset and peak latencies and dipole moment of the initial cortical activity estimated from the ECOG source waveforms in the ECOG study with six animals and onset latencies of the initial component of the evoked LFP for the R1 stimulation in the LFP experiment with nine animals. As for the snout stimulation, the pattern of the onset latencies is quite consistent with the pattern determined with the intracortical LFP. The differences in the onset latencies based on the ECOG and LFP data were quite small, comparable to the errors of estimates: Right R2 = +1.4 msec, Right SII = +2.2 msec, Left R1 = +1.4 msec, and Left SII = -0.6 msec, with the plus sign indicating a longer latency for the ECOG source estimates. These differences were not significant (*t*-test, $p > 0.025$).

Figure 8 summarizes the cortical projection map from the snout and forward connectivity map for R1. In addition to showing the nodes of the two networks, it shows the latency of connection from the snout to each projection site and latency of forward connection from R1. The estimates based on the LFP are shown in black, whereas those based on ECOG data are shown in green. The connection from the snout to the ipsilateral R1 is not shown since it was weak and not seen in 4/6 animals. As pointed out in Table 1, the latency estimates based on ECOG and LFP are very close to each other, especially for the contralateral dominant sources. Similarly, the latency estimates based on ECOG and LFP are very similar to each other for the forward connectivity from the R1 to other areas of the network.

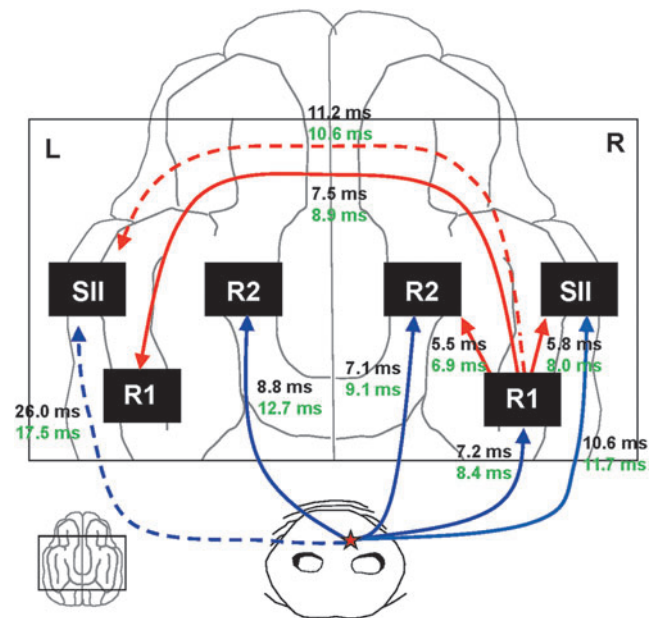


FIG. 8. Summary of the cortical connectivity maps in the swine somatosensory cortex. Thick arrows indicate hypothesized direct forward connections. Dotted lines indicate probable indirect connections. Mean onset latency is shown for each pathway. Right R1 area provides direct forward connections to right R2 and SII and left R1, but not R2. The homotopic areas of left and right R1 appear to be bidirectionally connected. Snout projects to right R1, R2, and SII and left R2 and SII, but not left R1. The onset latencies of evoked responses are very similar based on ECOG (green) and intracortical LFP (black).

Discussion

This study evaluated the capabilities and limitations of multiple dipole source analysis based on ECOG data for source estimation by comparing the estimates against results directly based on intracortical LFP. The comparisons were made for the effective projection from the trigeminal nerve to the somatosensory cortex and for a corticocortical effective connectivity. Although the number of activated sites detected with the ECOG was variable across animals, the cortical areas when they were activated were similar in location to those identified with the intracortical LFP for both the snout and R1 stimulations.

According to ECOG, the snout projected to all six areas of the somatosensory cortex across the group of animals, although some projections were seen only in a small number of animals and strength of activation was weak. The left snout stimulation strongly activated the contralateral right R1, R2, and SII, consistent with previous results (Craner and Ray, 1991a; Okada et al., 1999). The bilateral activation of R2 and SII was also consistent with the previous findings. These projections are largely consistent with the results based on intracortical LFP.

However, there was some inconsistency between the ECOG and LFP results. According to the ECOG source analysis, the snout stimulation activated the ipsilateral left R1. On the other hand, we could not detect any clear polarity reversal in the intracortical LFP measured in this area. In general, the polarity reversal indicates an active region, but lack of polarity reversal does not indicate the tissue to be inactive. For example, a pair of current sink and source may not be easily detectable when the basal dendrites are preferentially activated since this leads to an extracellular current source near the soma with weak, distributed sinks around the dendrites (Bollimunta et al., 2008; Schroeder et al., 1995). In the present case, this possibility appears unlikely. First, the projection from the snout to the contralateral R1 produces a pair of current dipoles based on a current source density (CSD) analysis, one in layer II/III and another in layer V, with multiunit activity distributed throughout cortical layers (Ikeda et al., 2005). Although we do not have a CSD profile for the projection to the ipsilateral R1, this previous result suggests that the stimulation may produce dipolar current distributions. Second, the fact that the projection from the snout to the ipsilateral R1 produced detectable peaks in the Laplacian maps based on the ECOG data in 2/6 animals indicates that at least in some cases the stimulation produced a dipolar laminar distribution. The location of peak activity for snout stimulation matched for ECOG and LFP when the activity was seen clearly with these two techniques. Thus, polarity reversal should have been seen with LFP. The reasons for this discrepancy between the ECOG and LFP data may be that the ECOG response was seen in left R1 only in 2/6 animals, its onset latency was quite long (14.7 ± 6.4 msec), and its moment was close to the variability of data (1.8 ± 0.8 nAm). The weak ECOG amplitude and lack of polarity in the LFP measurements suggest that the projection from the snout to the ipsilateral R1 was weak. This conclusion is consistent with the predominant contralateral projection from the snout to the R1 found earlier by Craner and colleagues (1991a).

The corticocortical connectivity map based on ECOG source analysis was practically identical to the map based

on intracortical LFP. According to ECOG, the right R1 was connected to the R1 itself and right R2 and SII and left R1 and SII. There was some weak peak seen in left R2, but the activity was too weak for reliable dipole analysis. The poor connection from right R1 to left R2 is consistent with the lack of clear polarity reversal of the intracortical LFP in this area. The agreement between the ECOG and LFP results for the projection from right R1 to left R2 supports our conclusion above that the projection from the snout to the ipsilateral R1 is weak.

Anatomical studies in other mammalian species indicate that there is a network of corticocortical connectivity among subareas in SI and SII corresponding to the maps found for the swine. SI sends homotopic callosal projections to the contralateral SI (Henry and Catania, 2006; Killackey et al., 1983; Manzoni et al., 1986), heterotopic callosal projections to the contralateral SII (Jones et al., 1979; Manzoni et al., 1986), and heterotopic association projections to the ipsilateral SII (Friedman et al., 1986; Henry and Catania, 2006; Manzoni et al., 1979). These results are consistent with the present result for the swine.

In addition to position information, the source analysis of ECOG data also provided latency information. The latencies of initial cortical activation estimated with the ECOG source waveforms were remarkably similar to those determined with the intracortical LFP, the latency differences being statistically all nonsignificant. The discrepancies in mean latency for these two estimates for snout stimulation were 1.1–2.0 msec (contralateral hemisphere) and 3.9–8.5 msec (ipsilateral hemisphere). The discrepancies for R1 stimulation were 1.4–2.2 msec for the ipsilateral and 0.6–1.4 msec for the contralateral hemisphere.

Some interesting similarities and differences found in this study are noteworthy. First, the peripheral projection from the snout to the ipsilateral R1 was weak or inconsistent according to both the ECOG and LFP data. In contrast, the projection from one R1 to the other R1 was quite clear and consistent (4/6 for ECOG and 9/9 for LFP) with a very short latency (8.9 ± 1.8 msec compared with 8.0 ± 0.3 msec for the ipsilateral SII). The short-latency response between the homotopic R1s suggests that the connection is transcallosal in swine. In some mammals, SI representing midline body structures has dense callosal connections, whereas callosal connections in SI for distal limb zones are sparse or absent (Ebner and Myers, 1962; Manzoni et al., 1989). In other mammals, however, the callosal connections between the SIs are sparse for midline body structures, for example, vibrissae in squirrels and rabbits (Gould and Kaas, 1981; Krubitzer et al., 1986; Ledoux et al., 1987). The barrel cortices in mice and rats have no callosal connections; instead, dense callosal connections are developed between disgranular cortices (Barth et al., 1994). It appears that in the case of swine there is a clear transcallosal connection between the homotopic areas of SI representing the snout. Thus, the converging input is absent from the periphery to the ipsilateral R1 and from the R1 on the opposite side to the same R1.

Second, the peripheral projection from the snout to the ipsilateral R2 was reliable (3/6 for ECOG and 3/4 for LFP). In contrast, the cortical connectivity from right R1 to left R2 was weak with no clear polarity reversal based on both the ECOG and LFP data. This contrasting result is an interesting example of asymmetry in the cortical network. In this case

the converging input is lacking in the R2 from the ipsilateral snout and the contralateral R1.

Third, a within-subject comparison of the two types of projection patterns led us to conclude that the location in the right R1 receiving the maximum projection from the snout projects to those areas that are indistinguishable from the areas receiving projections directly from the snout stimulation when a given projection area receives input from both pathways. In other words, there is convergence in information from the periphery and a cortical area to each projection site receiving input from these two areas. The lack of convergence of input in some areas and the presence of convergence in other areas may be important for understanding the information processing in the network.

The results from the present study overall indicate that the Laplacian mapping technique and multiple dipole source analysis of ECOG data provide valid estimates of the projection pattern from the periphery and corticocortical connectivity map. However, some cautions are needed in using these techniques for estimating effective connectivity in general. Although the dipole source analysis was able to accurately estimate the effective connectivity maps, such an analysis may be subject to some potential pitfalls. Activation of the snout or a cortical area did not always produce activation in all the nodes of the network identified with the group analysis. The number of projection areas was 2–5 for the snout stimulation and 1–5 for the R1 stimulation depending on the animal for the ECOG source estimation technique. The number of activated areas was also variable for the intracortical LFP, although less variable. The snout stimulation activated 3–5 areas in the 4 animals studied in one experiment. The R1 stimulation activated 4–5 areas in all 9 animals in another experiment. We do not know the basis for this variability. When a given area was activated, however, that area was consistent across the animals. Similar variability may be observed in other connectivity studies.

As another potential pitfall, source localization may yield biased results when a multiple dipole model is used to fit ECOG data over the entire electrode array in one step. This was especially the case when there was a dominant activity in one area—in this case, the right R1 receiving the projection from the left snout. The source localization was more accurate when the dipole location was first determined from the peak in the Laplacian map of the ECOG data, and then a multiple dipole model was used to fit all the data from the entire electrode array, leaving the source amplitude, orientation, and waveform free to vary. This is essentially the technique successfully used by Salmelin (2007) and Salmelin and associates (1994) in their language study with MEG.

Conclusions

The multiple dipole source analysis technique based on ECOG appears to be quite useful for estimating effective connectivity maps in the brain, including both position and latency of connectivity, although there are some potential pitfalls. The effective connectivity maps in the swine verified with intracortical LFP could be useful for evaluating the capabilities and limitation of other macroscopic techniques such as EEG, MEG, fMRI, and TMS-EEG for estimating functional cortical connectivity.

Acknowledgments

This study was supported by NIH Grants R01-NS21149 (Y.O.) and R01-NS30968 (Y.O.). We thank Dr. Isao Hashimoto for his encouragement throughout this project.

Author Disclosure Statement

No competing financial interests exist.

References

- Barth DS, Kithas J, Di S. 1994. The anatomic organization of evoked potentials in rat parietal cortex: electrically evoked commissural responses. *J Neurophysiol* 72:139–149.
- Blatow M, Nennig E, Durst A, Sartor K, Stippich C. 2007. fMRI reflects functional connectivity of human somatosensory cortex. *NeuroImage* 37:927–936.
- Bollimunta A, Chen Y, Schroeder CE, Ding M. 2008. Neuronal mechanisms of cortical alpha oscillations in awake-behaving macaques. *J Neurosci* 28:9976–9988.
- Brovelli A. 2012. Statistical analysis of single-trial Granger causality spectra. *Comput Math Methods Med* 2012:697610.
- Brovelli A, Ding M, Ledberg A, Chen Y, Nakamura R, Bressler SL. 2004. Beta oscillations in a large-scale sensorimotor cortical network: directional influences revealed by Granger causality. *Proc Natl Acad Sci USA* 101:9849–9854.
- Craner SL, Ray RH. 1991a. Somatosensory cortex of the neonatal pig: I. Topographic organization of the primary somatosensory cortex (SI). *J Comp Neurol* 306:24–38.
- Craner SL, Ray RH. 1991b. Somatosensory cortex of the neonatal pig: II. Topographic organization of the secondary somatosensory cortex (SII). *J Comp Neurol* 306:39–48.
- David O, Guillemain I, SAILLET S, Reyt S, Deransart C, Segebarth C, Depaulis A. 2008. Identifying neural drivers with functional MRI: an electrophysiological validation. *PLoS Biol* 6:2683–2697.
- David O, Kiebel SJ, Harrison LM, Mattout J, Kilner JM, Friston KJ. 2006. Dynamic causal modeling of evoked responses in EEG and MEG. *NeuroImage* 30:1255–1272.
- Ebner FF, Myers RE. 1962. Corpus callosum and the interhemispheric transmission of tactual learning. *J Neurophysiol* 25:380–391.
- Fox MD, Halko MA, Eldaief MC, Pasqual-Leon A. 2012. Measuring and manipulating brain connectivity with resting state functional connectivity magnetic resonance imaging (fcMRI) and transcranial magnetic stimulation (TMS). *NeuroImage* 62:2232–2243.
- Friedman DP, Murray EA, O'Neill JB, Mishkin M. 1986. Cortical connections of the somatosensory fields of the lateral sulcus of macaques: evidence for a corticolimbic pathway for touch. *J Comp Neurol* 252:323–347.
- Friston K. 2009. Causal modelling and brain connectivity in functional magnetic resonance imaging. *PLoS Biol* 7:220–225.
- Friston KJ, Harrison L, Penny W. 2003. Dynamic causal modeling. *Neuroimage* 19:1273–1302.
- Gould HJ 3rd, Kaas JH. 1981. The distribution of commissural terminations in somatosensory areas I and II of the grey squirrel. *J Comp Neurol* 196:489–504.
- Gross J, Timmermann L, Kujala J, Dirks M, Schmitz F, Salmelin R, Schnitzler A. 2002. The neural basis of intermittent motor control in humans. *Proc Natl Acad Sci USA* 99:2299–2302.
- He B, Yang L, Wilke C, Yuan H. 2011. Electrophysiological imaging of brain activity and connectivity—challenges and opportunities. *IEEE Trans Biomed Eng* 58:1918–1931.

- Henry EC, Catania KC. 2006. Cortical, callosal, and thalamic connections from primary somatosensory cortex in the nakes mole-rat (*Heterocephalus glaber*), with special emphasis on the connectivity of the inciser representation. *Anat Rec Part A* 288A:626–645.
- Ikeda H, Leyba L, Bartolo A, Wang Y, Okada YC. 2002. Synchronized spikes of thalamocortical axonal terminals and cortical neurons are detectable outside the pig brain with MEG. *J Neurophysiol* 87:626–630.
- Ikeda H, Wang Y, Okada YC. 2005. Origins of the somatic N20 and high-frequency oscillations evoked by trigeminal stimulation in the piglets. *Clin Neurophysiol* 116:827–841.
- Jones EG, Coulter JD, Wise SP. 1979. Commissural columns in the sensory-motor cortex of monkeys. *J Comp Neurol* 188:113–135.
- Kiebel SJ, David O, Friston KJ. 2006. Dynamic causal modeling of evoked responses in EEG/MEG with lead field parameterization. *NeuroImage* 30:1273–1284.
- Killackey HP, Gould HJ 3rd, Cusick CG, Pons TP, Kaas JH. 1983. The relation of corpus callosum connections to architectonic fields and body surface maps in sensorimotor cortex of new and old world monkeys. *J Comp Neurol* 219:384–419.
- Krubitzer LA, Sesma MA, Kaas JH. 1986. Microelectrode maps, myeloarchitecture, and cortical connections of three somatotopically organized representations of the body surface in the parietal cortex of squirrels. *J Comp Neurol* 250:403–430.
- Kveraga K, Guman AS, Kassam KS, Aminoff EA, Hamalainen MS, Chaumon M, Bar M. 2011. Early onset of neural synchronization in the contextual associations network. *PNAS* 108:3389–3394.
- Ledoux MS, Whitworth RH Jr., Gould HJ 3rd. 1987. Interhemispheric connections of the somatosensory cortex in the rabbit. *J Comp Neurol* 258:145–157.
- Lin F-H, Hara K, Solo V, Vangel M, Belliveau JW, Stufflebeam SM, Hamalainen MS. 2009. Dynamic Granger-Geweke causality modelling with application to interictal spike propagation. *Hum Brain Mapp* 30:1877–1886.
- Logothetis NK. 2012. Intracortical recordings and fMRI: an attempt to study operational modules and networks simultaneously. *NeuroImage* 62:962–969.
- Manzoni T, Caminiti R, Spidalieri G, Morelli E. 1979. Anatomical and functional aspects of the associative projections from somatic area SI to SII. *Exp Brain Res* 34:453–470.
- Manzoni T, Conti F, Fabri M. 1986. Callosal projections from area SII to SI in monkeys: anatomical organization and comparison with association projections. *J Comp Neurol* 252:245–263.
- Manzoni T, Barbaresi P, Conti F, Fabri M. 1989. The callosal connections of the primary somatosensory cortex and the neural bases of midline fusion. *Exp Brain Res* 76:251–266.
- Ojemann GA, Ojemann J, Ramsey NF. 2013. Relation between functional magnetic resonance imaging (fMRI) and single neuron, local field potential (LFP) and electrocorticography (ECoG) activity in human cortex. *Front Hum Neurosci* 7:34.
- Okada YC, Lähteenmäki A, Xu C. 1999. Comparison of MEG and EEG on the basis of somatic evoked responses elicited by stimulation of the snout in the juvenile swine. *Clin Neurophysiol* 110:214–229.
- Salmelin R. 2007. Clinical neurophysiology of language: the MEG approach. *Clin Neurophysiol* 118:237–254.
- Salmelin R, Hari R, Lounasmaa O, Sams M. 1994. Dynamics of brain activation during picture naming. *Nature* 368:463–465.
- Schroeder CE, Steinschneider M, Javitt DC, Tenke CE, Givre SJ, Mehta AD, Simpson GV, Arezzo JC, Vaughan HG Jr. 1995. Localization of ERP generators and identification of underlying neural processes. *Electroencephalogr Clin Neurophysiol Suppl* 44:55–75.
- Shafi MM, Westover MB, Fox MD, Pasqual-Leone A. 2012. Exploration and modulation of brain network interactions with noninvasive brain stimulation in combination with neuroimaging. *Eur J Neurosci* 35:805–825.
- Stephan KE, Friston KJ. 2010. Analyzing effective connectivity with fMRI. *Rev Cogn Sci* 1:446–459.
- Varela F, Lachaux J-P, Rodriguez E, Martinerie J. 2001. The brainweb: phase synchronization and large-scale integration. *Nat Rev Neurosci* 2:229–239.

Address correspondence to:
Yoshio Okada
Department of Medicine
Boston Children's Hospital
300 Longwood Avenue
Boston, MA 02115

E-mail: yoshio.okada@childrens.harvard.edu